

Likelihood Filter for Cluster Detection

P. Schuecker and H. Böhringer

Max-Planck-Institut für extraterrestrische Physik, D-85748 Garching, Germany

Received ; accepted

Abstract. The likelihood filter for cluster detection introduced by Postman et al. is generalized by using standard procedures and models originally developed in the theory of point processes. It is shown that the filter formulae of Postman et al. can be recovered in cases where background fields dominate the number counts. The performance of the generalized method is illustrated by using Monte Carlo simulations and by analyzing galaxy distributions extracted from the COSMOS galaxy catalogue. The generalized method has the advantage of being less biased at the expense of some higher computational effort.

Key words: clusters: general – X-rays: clusters – cosmology: observations

1. Introducing Remarks

The analogy between filtering and object detection in point distributions was recognized since more than 25 years (e.g., Yashin 1970, Snyder 1972, Rubin 1972). Recent astronomical applications are given in, e.g., Dalton et al. (1994), Kawasaki et al. (1998), and Postman et al. (1996). In the latter project (Palomar Distant Cluster Survey, PDCS) clusters of galaxies are detected and their redshifts and richnesses are estimated by maximizing the excess of the galaxy number counts as a function of angular coordinate and apparent magnitude with respect to the foreground and background galaxy distribution. In the following both distributions are referred to as ‘background’ distribution. The algorithm is based on the assumption that the statistics are dominated by the background galaxy counts. In this ‘high-background approximation’ the expected large numbers of galaxies ensure the validity of a Gaussian approximation of the corresponding likelihood function (central limit theorem) which is maximized to find the clusters and their basic parameters. It can be shown that this type of maximization corresponds to the minimization of the error-weighted squared

differences between observed and modeled data (method of least squares, e.g., Barlow 1996, p. 93). All counting errors are attributed to Poisson noise in the background. The method outlined above is optimized in finding distant clusters where the approximations seem to be appropriate. In the following we describe a generalization of the PDCS filter where no *a priori* information about the contrast of the cluster distribution with respect to the background distribution is needed. We replace the Gaussian approximation of the likelihood function by an exact expression based on local Poisson distributions with position-dependent mean intensities guided by the projected cluster number density profile and by the luminosity function. A similar approach based on binned data was developed independently by Kawasaki et al. (1998). Their finally used likelihood function, however, differs from the one derived in the present paper.

The aim of the present investigation is to study a mathematically exact and general likelihood filter which can be further optimized and then applied to the detection and characterization of isolated galaxy clusters located in comparatively uniform background galaxy fields. We plan to apply the method to galaxy fields centered around flux-limited samples of X-ray sources, e.g., to the ROSAT-ESO-Flux-Limited X-Ray (REFLEX) Cluster Catalogue (Böhringer et al., in preparation). The algorithm can be applied, however, to a much broader class of detection problems. The REFLEX clusters have measured redshifts up to $z = 0.30$; a few exceptional cases have $0.30 < z < 0.50$. The bulk of the data is located in the range $0.02 < z < 0.15$. Within the REFLEX project, the filter can be used to compute statistical significances of cluster detections, and to estimate redshifts and richnesses of the optical counterparts. The redshift estimates could further support those cluster redshifts which are obtained spectroscopically with only small numbers of cluster galaxies. The richness estimates could give more information about selection effects introduced by the complex X-ray/optical survey process of the REFLEX project.

The approach is based on the assumption that the spatial and the magnitude distributions of the galaxies located in the direction of clusters can be modeled by a

marked inhomogeneous Poisson point process. The resulting likelihood function is given in a compressed analytic form using the concept of the likelihood ratio statistics (Sect. 2). It is shown that the PDCS filter can be recovered in cases where background number counts dominate the statistic (Appendix B). Some practical notes on the application of the filter are given in Sec. 3. In Sect. 4 the performance of the general method is illustrated by analyzing simulated data to measure possible statistical biases of the derived numerical estimators (very often maximum likelihood estimators are not unbiased; see, e.g., Ripley 1991, Sect. 4, and Barlow 1996, p. 84) and by analyzing subsamples of the COSMOS galaxy catalogue to test the methods under more realistic survey conditions. The results are summarized and the deviations from the idealized model assumptions are discussed in Sect. 5. All computations assume pressureless Friedmann-Lemaître world models with the Hubble constant, H_0 , in units of $h = H_0/(100 \text{ km s}^{-1} \text{ Mpc}^{-1})$, a negligible cosmological constant, and the deceleration parameter $q_0 = 0.5$.

2. General Model

The spatial distribution of the galaxies can be regarded as an inhomogeneous but in principle more or less random pattern of points, i.e., as a realization of a point process in mathematical terminology (Neyman & Scott 1952, Layzer 1956, see also Neyman 1961 and references therein). The point process can be considered either as a random set of discrete points or as a random measure, counting the number of points in a given region (method of counts-in-cells). The points may be distributed in a three-dimensional volume, in a two-dimensional patch on the celestial sky, in a magnitude space, etc.

2.1. Inhomogeneous Poisson Point Process

All distributions with random locations of points and with local density parameters guided by a *nonrandom* variable fall into the category of inhomogeneous Poisson point processes. This is the case for the inhomogeneous galaxy distribution seen in the direction of one galaxy cluster where the local more or less radial-symmetric variation of the projected galaxy number density profile plus the uniform background field are determined by the intensity $\lambda(x)$. The inhomogeneous Poisson point process is well-known in the theory of point processes (see, e.g., Cressie 1993, p. 650 and references therein). If we replace the deterministic variation of the density parameter by a *random* variable we enter the field of doubly stochastic Poisson processes (Cox processes, see, e.g., Stoyan, Kendall, & Mecke 1995, p. 154) which are the general types of point processes to characterize large-scale distributions of galaxies (e.g., a Gaussian random field combined with local Poisson point processes).

Let x_1, \dots, x_N be one spatial realization of a point process. The N points, all with different coordinates, are distributed within the total volume A . A useful quantity with a simple interpretation and a direct relation to powerful analytical tools provided by the theory of point processes is the local Janossy density, $j_N(x_1, \dots, x_N|A)$: after multiplication of $j(\cdot)$ with the product of the volume elements $dx_1 \cdots dx_N$ it gives the probability that in the total volume A there are exactly N points in the process, one point in each of the N distinct infinitesimal half-open regions $[x_i, x_i + dx_i)$. The Janossy density may be regarded as the likelihood L_A of the realization, ignoring – as usual – the principle differences between probability density functions and sample functions:

$$L_A(x_1, \dots, x_N) := j_N(x_1, \dots, x_N|A). \quad (1)$$

Assume that the number of galaxies observed per unit solid angle depends only on the spatial coordinate x and gives the intensity $\lambda(x)$. More complicated models where also the magnitudes of the galaxies are taken into account are discussed below in the context of marked point processes (see Sec. 2.2). The intensity $\lambda(x)$ is considered as the x -dependent density parameter of an inhomogeneous Poisson process.

The Janossy density and thus the likelihood function of the inhomogeneous Poisson point process can be derived directly by using the machinery of probability generating functionals and Khinchin measures (Daley & Vere-Jones 1988, p. 498). The application of this formalism offers, however, the possibility to derive likelihood functions for more complex point processes, e.g., multiple stochastic point processes which might be interested for many cosmological applications. A guideline through the basic equations of the formalism is given in Appendix A. For inhomogeneous Poisson point processes this standard formalism leads to the logarithmic likelihood (see also Snyder 1975, Karr 1986, and Appendix A)

$$\ln L_A = - \int_A \lambda(x) dx + \sum_{i=1}^N \ln \lambda(x_i). \quad (2)$$

Equation (2) can also be found in a more heuristic way. As already mentioned above, the quantity $L_A(x_1, \dots, x_N) dx_1 \cdots dx_N$ may be regarded as the probability of finding exactly one point in each of the infinitesimal volume elements dx_1, \dots, dx_N , (case a), whereas outside of these regions no further points are present, (case b). These events are independent, due to the independence properties of the Poisson process. The probabilities for (a) are given by $\lambda(x_i) dx_i$ (for each individual point), and the probability for (b) is given by the avoidance or void probability function, $\exp(-\int \lambda(x) dx)$. The integration extends over the volume A reduced by the sum of the infinitesimal volume elements, dx_i , which can be neglected due to their small size so that, in total, the integration extends over the complete volume A (Stoyan & Stoyan 1992, p. 258).

2.2. Inhomogeneous Marked Poisson Point Process

In order to generalize the model described above note that galaxy distributions can also be regarded as realizations of *marked* spatial point processes, each consisting of locations of events in a bounded study region A and associated measurements (marks). Typical marks, often found in cosmological applications are apparent magnitude, luminosity, mass, energy, color, morphological type, etc. In this case the realization of a marked point process is $(x_1, m_1), \dots, (x_N, m_N)$. We assume the absence of any segregation effects, i.e., that the marks are independent-and-identically-distributed and are independent of the associated marginal spatial point process. Define the point process by a counting measure on the product space $A \times B$ of two intervals with, for example, $x_i \in A \subset \mathbb{R}^3$, and $m_i \in B \subset \mathbb{R}^1$. The moment measures of a marked spatial point process are simple extensions of the moment measures of an ordinary spatial point process. The generalization of (2) to marked inhomogeneous Poisson point processes is thus straightforward and is given by

$$\ln L_{A \times B} = - \int_A \int_B \lambda(x, m) dm dx + \sum_{i=1}^N \ln \lambda(x_i, m_i) \quad (3)$$

Usually, $\lambda(x, m)$ can be factorized as $\lambda(x, m) = f(m|x) \cdot \lambda_0(x)$ where $f(m|x)$ is the conditional density of the marks, so that the log-likelihood can be maximized separately for the parameters characterizing f and λ_0 .

2.3. Application to Cluster Detection

In the case of finding clusters of galaxies using spatial and magnitude information $\lambda(x, m)$ cannot be factorized as can be seen from the model for the number of galaxies observed per unit area and per unit magnitude interval introduced by Postman et al. (1996),

$$\lambda(r, m) := b(m) + \Lambda \phi(m - m^*) P\left(\frac{r}{r_c}\right). \quad (4)$$

Here, $b(m)$ gives the differential magnitude number counts of the background galaxies, $\phi(m - m^*)$ is the luminosity function (e.g., in the Schechter prescription) of one cluster shifted along the apparent magnitude scale in accordance with the given redshift parameter and superposed onto the background distribution, $P(r/r_c)$ is the cluster angular surface number density profile as a function of the projected (radial) distance r from the center of the cluster with the projected characteristic radius r_c , and Λ is a dimensionless parameter characterizing the intrinsic cluster richness. Equation (4) assumes a uniform, i.e., unclustered background galaxy distribution, and that all clusters have the same luminosity function and the same spatial num-

ber density profile. For the model (4) with given $b(m)$, and the normalization (if the integrals do not diverge)

$$\int_A \int_B \phi(m - m^*) P\left(\frac{r}{r_c}\right) dm d^2r = 1, \quad (5)$$

equation (3) can be written as

$$\ln L = - \int_A \int_B b(m) dm d^2r - \Lambda + \sum_{i=1}^N \ln \left(b(m_i) + \Lambda \phi(m_i - m^*) P\left(\frac{r_i}{r_c}\right) \right). \quad (6)$$

It is convenient to normalize likelihood functions using the concept of likelihood ratio statistics. Further notes on the scope of adaptability of the likelihood ratio statistics, especially when not all random variables may be independent, can be found in Sen & Singer (1993, p. 72). For the present situation where $b(m)$ is assumed to be known the results do, however, not explicitly depend on the specific normalization. As a reference process in the denominator usually the homogeneous Poisson process is chosen. In order to get a likelihood ratio where its maximization explicitly maximizes the contrast between cluster and background, an inhomogeneous Poisson process with an r -independent density as given in (4) for $\Lambda = 0$ (background model) seems to be more appropriate. Note that although the point distribution of this specific model is homogeneous in the spatial domain it is still inhomogeneous in the magnitude space. The corresponding log-likelihood is

$$\ln L_0 = - \int_A \int_B b(m) dm d^2r + \sum_{i=1}^N \ln b(m_i). \quad (7)$$

With this normalization the final log-likelihood ratio is

$$\ln \left(\frac{L}{L_0} \right) = -\Lambda + \sum_{i=1}^N \ln \left(1 + \frac{\Lambda \phi(m_i - m^*) P\left(\frac{r_i}{r_c}\right)}{b(m_i)} \right). \quad (8)$$

The richness parameter Λ is obtained from the relation $\partial \ln(L/L_0)/\partial \Lambda = 0$, resulting in the condition:

$$\sum_{i=1}^N \frac{\phi(m_i - m^*) P\left(\frac{r_i}{r_c}\right)}{b(m_i) + \Lambda \phi(m_i - m^*) P\left(\frac{r_i}{r_c}\right)} = 1. \quad (9)$$

Equations (8) and (9) can be used for the detection of clusters in the following way: In the first step, values for m^* and r_c are selected so that, for given functional forms of ϕ and P , equation (9) gives the corresponding richness parameter using standard numerical root finding algorithms (see, e.g., Brent 1973, Sect. 3 and 4). In the second step, this Λ value is inserted into (8) where $\ln(L/L_0)$ serves as a significance measure for the detected cluster candidate. The relations between the observed and the distant-independent values of the filter parameters are determined

by the redshift z and the chosen cosmological model. The final cluster redshift and richness values are thus fixed by the z value with the highest log-likelihood ratio. From $\Lambda = 0$ it can be deduced that for a general galaxy field, $\ln(L/L_0) = 0$ is the mode of the distribution of the logarithmic values of the likelihood ratios. The distribution is asymmetric with a long tail to larger $\ln(L/L_0)$ -values where the rich clusters are expected. Approximations of the equations (8) and (9) are given in Appendix B.

3. Practical Considerations

For the application of the filter the intervals A and B in (5) must be specified. The following computations assume the half-open r - and m -ranges

$$A = [0, r_{\text{co}}), \quad B = [m_{\text{bright}}, m_{\text{faint}}). \quad (10)$$

In equations (10) r_{co} is the halo or cutoff radius defined by $P(r/r_c) = 0$ for $r \geq r_{\text{co}}$, and $P(r/r_c) > 0$ for $r < r_{\text{co}}$. The bright and the faint-end limit of the apparent magnitudes of the sample galaxies are m_{bright} and m_{faint} , respectively. For radial-symmetric cluster profiles, equations (10), (4), and (5) give a second estimator for the cluster richness,

$$\begin{aligned} \hat{\Lambda} &= 2\pi \int_0^{r_{\text{co}}} r \int_{m_{\text{bright}}}^{m_{\text{faint}}} \lambda(r, m) dm dr \\ &- 2\pi \int_0^{r_{\text{co}}} r \int_{m_{\text{bright}}}^{m_{\text{faint}}} b(m) dm dr = N_0 - N_{\text{bg}} = N_{\text{cl}}. \end{aligned} \quad (11)$$

With the specific choice (10), $\hat{\Lambda}$ is the difference between the total number of galaxies, N_0 , seen in the direction of the cluster, and the number of background galaxies, N_{bg} , expected for the cluster area determined by r_{co} . Therefore, $\hat{\Lambda}$ is a statistical measure of the number of cluster galaxies, N_{cl} , detected in the magnitude range B above the background distribution. The estimator gives richnesses which depend on cluster redshift. Note the difference between Λ defined as a parameter characterizing the intrinsic cluster richness by equation (4) without any constraints on the intervals A and B , and $\hat{\Lambda}$ defined as an estimator of the cluster richness through equation (11) under the constraints (10). Equation (11) not only shows that estimates of cluster richnesses obtained with (9) or (11) are biased. The equation also offers a new way to circumvent the more complicated estimation of Λ by solving condition (9). Richnesses obtained with (11) are, however, not obtained with the maximum likelihood principle. Therefore, the combination of $\hat{\Lambda}$ with (8) does not necessarily yield consistent maximum likelihood values.

A redshift-independent and thus unbiased estimate, Λ_0 , of the intrinsic cluster richness may be obtained from the ratios

$$\frac{\Lambda}{\Lambda_0} = \frac{\int_{m_{\text{bright}}}^{m_{\text{faint}}} \phi(m - m^*) dm}{\int_{m_{\text{bright}}}^{m_{\text{co}}} \phi(m - m^*) dm}$$

$$= \left[\int_{m_{\text{bright}}}^{m_{\text{co}}} \phi(m - m^*) dm \right]^{-1}, \quad (12)$$

where Λ is given by (9), and the cutoff magnitude, m_{co} , used as the upper limit of the numerical integration of the luminosity function, must be chosen in accordance with the cluster redshift. This magnitude may be defined by

$$m_{\text{co}}(z) := m^*(z) + \Delta m \text{ [mag]}. \quad (13)$$

Here, $m^*(z)$ is determined by the cluster redshift and $m_{\text{co}}(z)$ by a predefined increment, Δm magnitudes fainter than $m^*(z)$. The last equality in (12) uses the normalization (5) separately for the radial and for the magnitude profile:

$$\int_0^{r_{\text{co}}} P\left(\frac{r}{r_c}\right) 2\pi r dr = 1, \quad \int_{m_{\text{bright}}}^{m_{\text{faint}}} \phi(m - m^*) dm = 1.$$

The equations (12) can also be used to correct $\hat{\Lambda}$ for redshift biases. Finally, it should be noted that m_{bright} must be bright enough to include the brightest galaxy of the sample.

4. Filter Performance

The following computations illustrate the basic properties of the likelihood filter. The model is given by the equations (8), (9), (10), (12), and (13). All numerical simulations and reductions are performed for the photographic b_J passband. Observed data are taken from the COSMOS galaxy catalogue (e.g. Heydon-Dumbleton et al. 1989).

For the magnitude filter, ϕ , a Schechter-type luminosity function is used with the characteristic magnitude, $M^* = -20.1 + 5 \log h$ [mag], and the faint-end slope, $\alpha = -1.2$ (Colless 1989, Lumsden et al. 1997). The COSMOS magnitudes are corrected for the effect of the limited dynamic range within the microdensitometer ('saturation effect') as in Lumsden et al. (1997, Sect. 2.2). The cosmic ($K + E$) corrections for the b_J passband are parameterized as $K(z) = 3.0z$ [mag] (Efstathiou, Ellis, & Peterson 1988; Dalton et al. 1997). If the galaxy magnitudes have large random errors one has to replace $\phi(m - m^*)$ by the luminosity function convolved with the magnitude errors.

The corrections for galactic extinction are applied to observed data using the correlation between visual extinction and neutral Hydrogen column density, $N_H[\text{cm}^{-2}]/A_V = 1.79 \times 10^{21}$ (Predehl & Schmitt 1995). The visual extinctions are transformed to the B band using the colour excess $E_{B-V} = A_B - A_V$ and $A_B = 4.3E_{B-V}$ (de Vaucouleurs et al. 1991, p. 30). It is assumed that the extinction in the B band closely resembles the effect in the b_J passband. Hydrogen column densities are taken from Dickey & Lockman (1992) as provided by the EXSAS97 release.

For the radial filter, P , a King-like profile as given in Postman et al. (1996) is used,

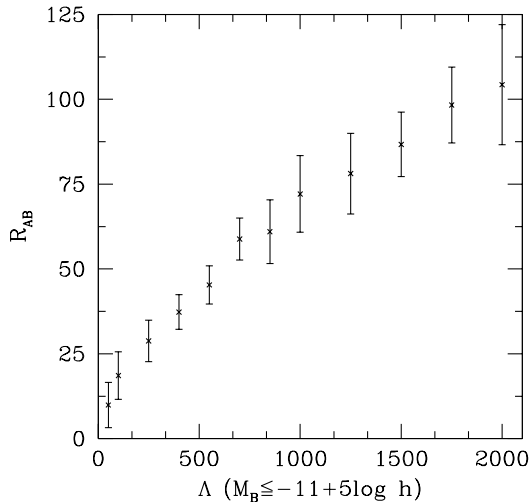


Fig. 1. Abell cluster richness R_{AB} determined from simulations as a function of the intrinsic cluster richness Λ , i.e., the number of cluster galaxies (above background) with (as an example) absolute magnitudes $M \leq -11 + 5 \log(h)$ [mag]. The 1σ error bars are the standard deviations obtained from simulations of clusters at different redshifts. The simulations give galaxy distributions as expected from the COSMOS galaxy catalogue.

$$P(b) = \begin{cases} (1 + b^2)^{-\frac{1}{2}} - (1 + C^2)^{-\frac{1}{2}} & : b < r/r_{co} \\ 0 & : b \geq r/r_{co} \end{cases},$$

with $b = r/r_c$ and $C = r_{co}/r_c$. The core radius and the cutoff radius have the respective values $r_c = 100h^{-1}$ kpc and $r_{co} = 1h^{-1}$ Mpc. For the richness estimates using equation (12) the magnitude increment $\Delta m = 3.0$ mag in (13) was chosen.

In the following paragraphs the detection of individual clusters and the estimation of cluster richnesses are discussed (Sect. 4.1). For *rich* clusters the likelihood filter derived in Sections 2 and 3 gives unbiased estimates of the cluster redshift, as illustrated by the application of the filter to simulated data (Sect. 4.2) and to observed data (Sect. 4.3).

4.1. Cluster Richness and Cluster Detection from Simulations

Although not essential for the application of the likelihood filter, knowledge of the relation between the traditional Abell cluster richness, R_{AB} , and the not observable intrinsic cluster richness, Λ , defined by equation (4) is helpful in order to understand the efficiency of cluster detection and cluster characterization. Isolated clusters with known redshifts, equatorial coordinates, and richnesses, superposed onto an homogeneous background galaxy distribution, are

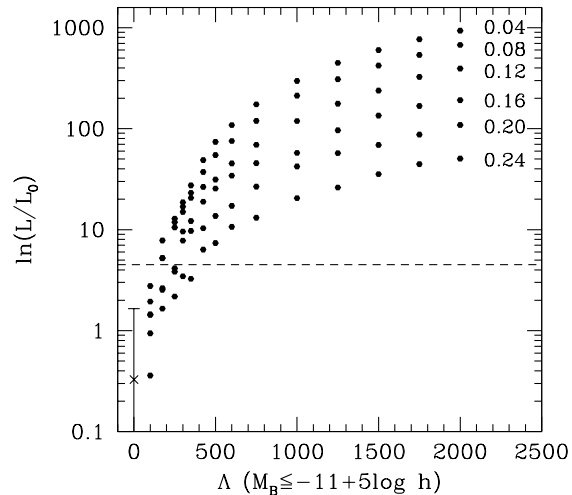


Fig. 2. Log-likelihood ratios for clusters (points) simulated with intrinsic richnesses $100 \leq \Lambda \leq 2000$ in the redshift range $0.04 \leq z \leq 0.24$, marked on the right-end of each sequence. The short-dashed line shows the (formal) 3σ detection limit. The vertical error bar at zero richness indicates the 3σ range of the $\ln(L/L_0)$ values obtained for simulated fields without superposed clusters of galaxies.

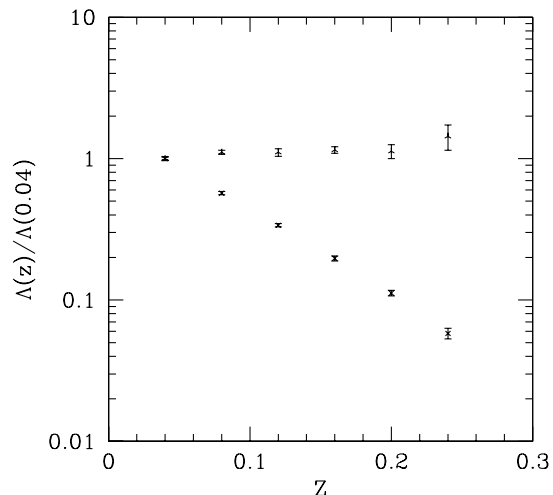


Fig. 3. Richness estimates Λ (declining sequence) and Λ_0 (horizontal sequence) as a function of redshift z from simulated clusters of galaxies. Richnesses Λ are computed with equation (9); richnesses Λ_0 are computed with equation (12). Both richness estimates are normalized at $z = 0.04$. The error bars correspond to the 1σ standard deviations. The errors are comparatively small because of the high richness ($\Lambda = 2000$) used in the simulations.

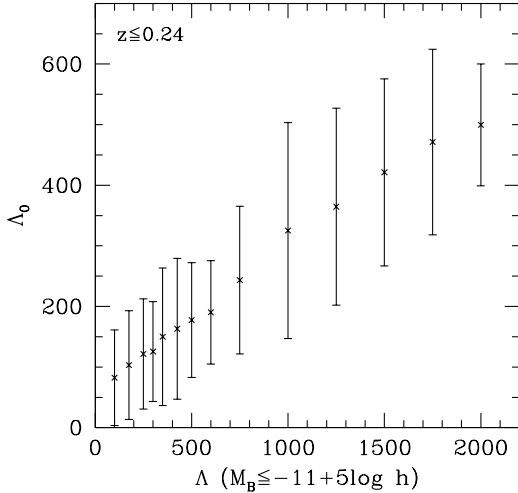


Fig. 4. Richness estimates Λ_0 obtained with the likelihood filter from simulated clusters with redshifts $z \leq 0.24$ as a function of intrinsic richness Λ (defined by equation 4). Error bars correspond to 1σ standard deviations.

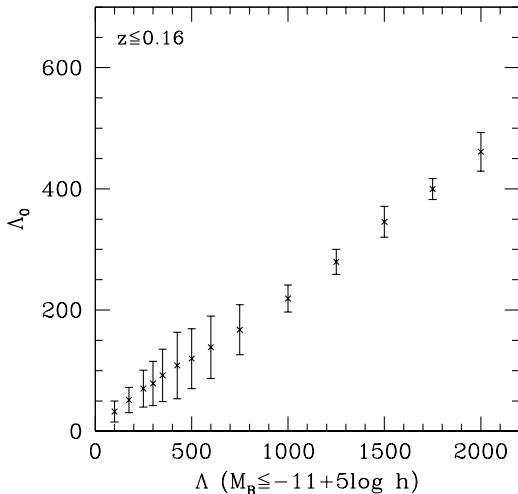


Fig. 5. As Fig. 4 for clusters with redshifts $z \leq 0.16$.

simulated with simple Monte Carlo methods in relativistic spacetime. The galaxies have apparent magnitudes in the range $0.0 \leq b_J \leq 20.5$ mag. The background number counts, $b(m)$, are guided by polynomial fits to the differential distributions collected by Metcalfe et al. (1993). The luminosity functions and the projected radial number density profiles of the simulated clusters are the same as those used in the likelihood filter. The results obtained from numerical simulations are shown in Fig. 1. For each intrinsic

richness Λ , the mean Abell richnesses (crosses) and the 1σ error bars are obtained from clusters simulated at different redshifts. The analysis concentrates on the Abell richness classes $-1, 0, 1$, and 2 because most of the clusters we want to study have these comparatively low richnesses. The nonlinearity between the R_{AB} and the Λ richnesses as seen in Fig. 1 is introduced by the richness-dependency of m_3 , that is, the apparent magnitude of the 3rd-brightest cluster galaxy (Scott effect). The large scatter of the individual richness estimates is mainly caused by the large scatter of the m_3 values.

Figure 2 shows the efficiency of the likelihood filter for cluster detection as a function of the intrinsic cluster richness Λ and for different cluster redshifts, given at the right-end of each sequence in the figure. The 3σ range of the $\ln(L/L_0)$ values obtained for pure background fields without superposed galaxy clusters is indicated by the vertical error bar at $\Lambda = 0$. As expected, the log-likelihood values increase with increasing cluster richness and decreasing cluster redshift. The simulations suggest that if the clusters have the same luminosity function and radial number density profile as used in the likelihood filter then the method would detect all clusters in the COSMOS galaxy catalogue with redshifts $z \leq 0.24$ and richness $\Lambda \geq 500$ or $R_{AB} > 40$ (Abell richness class 0) on significance levels $\geq 3\sigma$. For larger redshifts, however, only clusters with larger richnesses can be detected.

The richness estimates Λ obtained with equation (9) and the richness estimates Λ_0 obtained with (12) are compared in Fig. 3. As shown in Sect. 3, Λ estimates are always redshift-dependent when they are computed within fixed magnitude intervals. They give the number of cluster galaxies above the background field: this number decreases with increasing z . Contrary to this, Λ_0 estimates are corrected for the effect of the redshift-dependent magnitude range of the cluster galaxies. These estimates are almost constant over the given z interval.

The accuracies of richness estimates are always limited by principle problems concerning the determination of the cluster memberships and by the small numbers of detectable galaxies in distant clusters. These problems are illustrated in the Figs. 4 and 5. The richness estimates Λ_0 are computed for clusters at different redshifts and intrinsic cluster richnesses Λ . The number of simulated clusters is constant per unit redshift interval. As expected, the random errors of the Λ_0 estimates increase significantly for poor clusters at high z . Moreover, cluster richnesses are systematically overestimated for samples with high z . Only for cluster samples with small z and high Λ we can expect unbiased estimates which are directly linked to the intrinsic cluster richnesses.

4.2. Tests for Redshift Biases from Simulations

The following tests are devoted to studies concerning possible systematic redshift errors which might be inherent

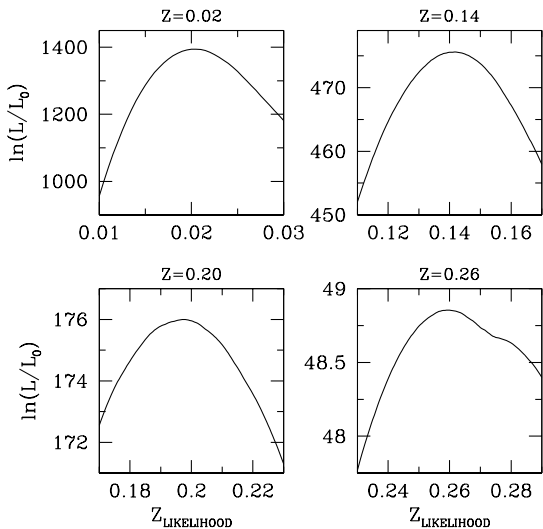


Fig. 6. Examples of log-likelihood curves from simulated data. The intrinsic richness of the clusters is $\Lambda = 10^4$. The redshifts of the clusters are given on top of each panel. Formal standard deviations of the redshift estimates can be obtained from the points where the log-likelihood curve has fallen by 0.5 (1σ), 2.0 (2σ), 4.5 (3σ), ... from its maximum.

for the derived method. In order to detect z biases without the disturbing effects of the discreteness noise, the analysis begins with the simulations of clusters with high intrinsic richnesses, $\Lambda = 10^4$. We regard these simulations as some kind of numerical integration of the relevant equations. At the end of this paragraph, the results from the simulations of clusters with low richnesses are discussed.

Figures 6 show the likelihood values obtained for four rich clusters simulated at the redshifts $z = 0.02, 0.14, 0.20$, and 0.26 . As already shown in the preceding sections, the magnitude and redshift ranges of these simulations give galaxy distributions as selected from the COSMOS galaxy catalogue.

For all redshifts the log-likelihood curves in Fig. 6 peak close to the true cluster redshifts (indicated on top of each panel). For intermediate z values, the comparatively high symmetry of the curves around the correct cluster redshift indicates the absence of large systematic z errors. For small and for large redshifts the curves get more asymmetric. This might be taken as a hint to possible increasing systematic z errors when the method is applied to comparatively nearby or distant clusters.

The asymmetries, however, do not significantly affect the positions of the maxima of the log-likelihood curves and thus of the derived redshifts. For example, the differences, Δz , between the true redshifts and the likelihood redshifts are $|\Delta z| = 0.0005$ for the extreme redshifts $z = 0.02$ and $z = 0.26$, and do not exceed $|\Delta z| = 0.0025$ for all cases studied so far. For very rich clusters, the Δz

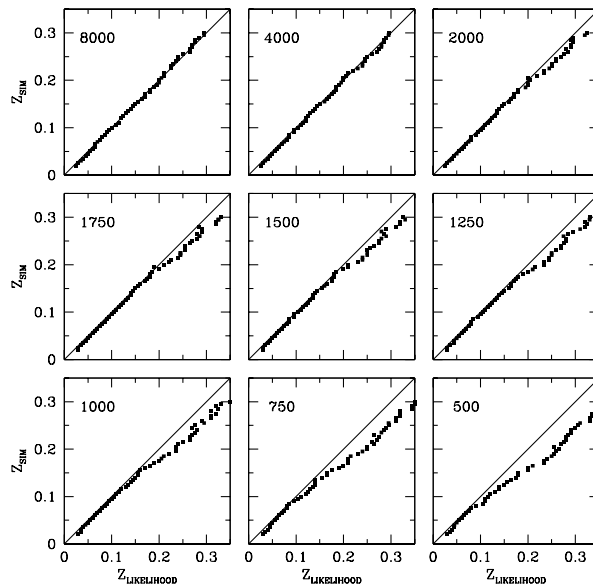


Fig. 7. Comparison of the redshift estimates obtained with the likelihood filter, $z_{\text{Likelihood}}$, with the true cluster redshifts, z_{SIM} , for different intrinsic cluster richnesses (Λ value given in the upper left of each panel). The data are obtained from simulations. The richness $\Lambda = 8000$ corresponds to a very rich cluster whereas $\Lambda = 500$ characterizes a cluster which is near the detection limit of the likelihood filter expected for the simulated COSMOS data when the cluster is located at $z \approx 0.24$.

values do not show any z -dependent trends, and are of the order of the expected numerical accuracies.

We thus conclude that numerical studies under ideal conditions (high richness, and background distribution assumed to be known) give no indications for possible z -dependent biases of the locations of the maxima of the log-likelihood curves.

The situation changes for poor clusters and when the background number counts must be estimated from the sample itself. The comparison of the likelihood redshifts with the true cluster redshifts is shown for different intrinsic richnesses in Fig. 7. For high richnesses no systematic redshift errors are detected, supporting the results of the analyses described above. For poor clusters with, e.g., $\Lambda = 500$ (i.e., clusters close to the detection limit at $z = 0.24$) a systematic overestimation of z at high redshifts is found. This is mainly caused by the small number of cluster galaxies detected for poor clusters at high z leading to a systematic undersampling of the bright end of the cluster luminosity function and of the outskirts of the projected cluster profile.

4.3. Redshifts from Observed Data

Before we describe the results obtained with the likelihood filter on observed data a few comments regarding some practical limitations are given. The derivation of the like-

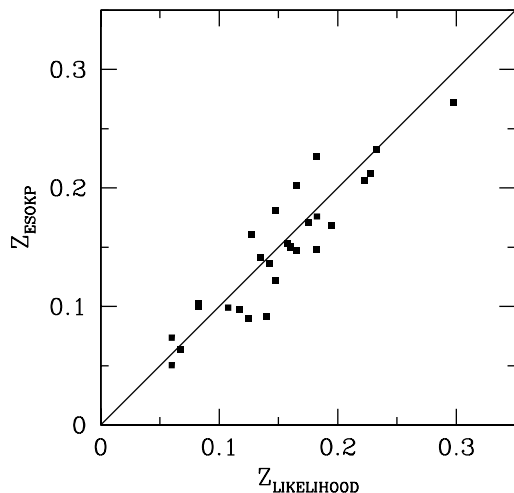


Fig. 8. Redshifts of observed clusters of galaxies, $Z_{\text{LIKELIHOOD}}$, obtained with the likelihood filter using subsamples of the COSMOS galaxy catalogue, and spectroscopic cluster redshifts, Z_{ESOKP} , obtained with eight to 20 galaxies per cluster as published in the REFLEX catalogue of Böhringer et al. (in preparation).

likelihood filter rests on the assumption of an homogeneous and isotropic spatial distribution of the background galaxies. In mathematical terminology this involves the validity of first-order motion invariance, i.e., the invariance of the mean intensity of galaxies in the study area outside the cluster region under spatial translations and rotations. In many practical situations the observed data do not fulfill these requirements.

On small scales, the galaxy field is strongly clustered so that comparatively large solid angles are needed to reduce biases in the background determination. On large scales, extreme care must be taken to achieve homogeneous sampling of the galaxy field. The latter aspect is important for the analysis of galaxy catalogues obtained from mosaics of digitized Schmidt plates where the effects of vignetting, desensitization, and small errors in magnitude zero-points may introduce artificial fluctuations in the observed galaxy field, especially when galaxy distributions obtained from different plates are combined. For the application of the likelihood filter to observed data it is thus necessary to extract galaxy fields on areas which are not too small to be affected by galaxy number density fluctuations and which are not too large to be affected by artificial plate-to-plate variations.

Tuckey’s median polishing offers a robust way to detect large-scale deviations from first-order motion invariance in point distributions. The algorithm successively subtracts medians out of rows of gridded data (number counts in quadratic cells), then columns, then rows, then columns, and so on, accumulating them in ‘row’, ‘column’, and ‘all’

registers, and leaves behind the table of residuals. The convergence of this procedure is discussed in Kemperman (1984). An illustration of the algorithm is given in Appendix C.

We use this algorithm after transforming the equatorial object coordinates into Hammer-Aitoff equal-area coordinates to flag regions by searching for cells in the row and in the column registers which significantly deviate ($> 5\sigma$ formal background noise) from the mean galaxy background distribution and exclude the corresponding plates from further analyses. The results obtained with median polishing sometimes strongly depend on the specific orientation of the row and column axes. Therefore, we apply the algorithm using three different orientations. For each orientation, median polishing usually converges after three to five iterations. The iteration stops when the relative changes between two successive iteration steps are less than one percent.

In Fig. 8 the redshift estimates obtained with the likelihood filter on subsamples of the COSMOS galaxy catalogue are compared to cluster redshifts obtained from spectroscopic observations. The central cluster coordinates and the cluster redshifts are taken from the REFLEX catalogue (Böhringer et al., in preparation). The test sample includes 43 REFLEX clusters observed among others within the ESO Key Programme (e.g., Guzzo et al. 1995). These clusters have redshifts determined with eight to 20 cluster galaxies and are thus well-suited as redshift references. In addition, the presence of comparatively strong X-ray signals from these sources and the absence of active galaxies further support the existence of real clusters in these areas. The test sample is not a representative subsample of the complete REFLEX catalogue. It is biased to larger redshifts because the complete REFLEX sample includes also a large number of nearby clusters.

All COSMOS galaxies with $b_J \leq 20.5$ mag (after correction for saturation effects and galactic extinction) located within spherical regions of about two degrees radius around the X-ray cluster positions are selected. After median polishing and careful determination of the bright and of the faint magnitude limits of the galaxies in each study region, typically 10 000 galaxies (background + cluster) remain per cluster target.

For 28 clusters from the list of 43 test clusters the filter detects a maximum in the likelihood functions within the redshift range $0.0 \leq z \leq 0.35$. The parameters of the likelihood filter are the same as used in the simulations. The corresponding $Z_{\text{LIKELIHOOD}}$ values are shown in Fig. 8. For the remaining 15 test clusters no redshifts could be determined, either because of their weak statistical significance $\ln(L/L_0) < 4.5$ (two cases) or because no local maximum was detected (13 cases). These redshift incompletenesses increase with increasing redshift from 20 to 25 percent for $z < 0.2$ to 53 percent for $z > 0.2$. However, the redshift distribution of the test clusters was

Table 1. Effects of false M^* and r_{co} filter parameters on redshift and richness estimates. M^* values are given in units of $5 \log(h)$ mag, r_{co} values are given in units of Mpc/h (see text).

$M^* r_{\text{co}}$	0.5	1.0	2.0
-18.1	0.050 1033	0.075 2080	0.090 3029
-20.1	0.064 433	0.109 986	0.148 1754
-22.1	0.065 206	0.131 425	0.240 1090

Table 2. Effects of false M^* and r_c filter parameters on redshift and richness estimates. M^* values are given in units of $5 \log(h)$ mag, r_c values are given in units of Mpc/h (see text).

$M^* r_c$	0.05	0.1	0.5
-18.1	0.070 1835	0.075 2080	0.085 2638
-20.1	0.106 921	0.109 986	0.120 1121
-22.1	0.128 420	0.131 425	0.140 457

Table 3. Effects of substructure on the richness and redshift estimates as a function of the separation Δr and for different richness ratios Λ_1/Λ_2 of the two components. The application of the general likelihood filter gives the normalized richness (numerator) and the redshift (denominator) for the combined system.

$\frac{\Delta r}{r_c} \frac{\Lambda_1}{\Lambda_2}$	1.000	0.500	0.250	0.125	0.025	0.000
0	2.059 0.104	1.529 0.105	1.265 0.105	1.130 0.106	1.026 0.106	1.000 0.106
1	2.049 0.104	1.525 0.105	1.409 0.105	1.259 0.106	1.025 0.106	1.000 0.106
2	2.043 0.101	1.517 0.104	1.255 0.105	1.257 0.106	1.025 0.106	1.000 0.106
3	2.023 0.102	1.505 0.105	1.246 0.104	1.122 0.105	1.024 0.105	1.000 0.106
5	1.759 0.095	1.464 0.103	1.229 0.101	1.110 0.104	1.022 0.105	1.000 0.106
7	1.511 0.104	1.254 0.102	1.188 0.096	1.086 0.101	1.016 0.106	1.000 0.106

constructed to be almost redshift-independent so that the given incompleteness values must be weighted with the *a priori* probabilities for the presence of clusters of galaxies within different redshift intervals (multiplication formula for probabilities). Therefore, the actual incompletenesses are expected to be much smaller compared to the values given above. The standard deviation of the redshift differences ($Z_{\text{LIKELIHOOD}} - Z_{\text{ESOKP}}$) is $\sigma_z = 0.023 \pm 0.004$.

5. Concluding Remarks

Both the PDCS filter and the generalized filter derived in the present paper give systematic redshift errors for clusters at high z . The generalized filter overestimated redshifts at high z ; the errors tend to zero for richer systems. The PDCS underestimates redshifts at high z ; the errors tend to zero for richer systems (see Fig. 14 in Postman et al.). Whereas the errors of the generalized method can be explained by the incomplete sampling of the filter profiles for poor clusters at high z , the errors of the PDCS filter can not be judged in an easy way. Reasons for the discrepancies between the two methods are still not clear because of the complexity of the PDCS approximations. Nevertheless, it seems that if one uses the exact mathematical equations, as does the generalized method, corrections like the ‘cluster signal correction’ of the PDCS filter are not necessary.

It is shown that the richness estimates obtained with the generalized filter are redshift-dependent and must be corrected (e.g., with equation 12). It is not clear why similar corrections are not necessary for the PDCS filter.

Similar conclusions about the PDCS filter are drawn by Kawasaki et al. (1998). In contrast to the generalized method, the Kawasaki filter uses binned data and does not maximize the contrast between field and cluster galaxy counts. A detailed comparison of the generalized method and the approximations introduced by Kawasaki et al. is in preparation.

The final question concerns the validity of the chosen assumptions used to derive the likelihood filters. Problems caused by deviations of the spatial distribution of the background galaxies from the assumed uniform distribution were already discussed in Sect. 4.3.

Further systematic errors in the derived cluster redshifts and richnesses arise when the luminosity functions and the number density profiles of the likelihood filter do not match with the corresponding functions of the observed clusters. As an example, Tabs. 1 and 2 illustrate the effects of false filter parameter values M^* , r_{co} , and r_c on the estimates of z and Λ_0 . The results are obtained from simulated data. The ‘correct’ cluster parameters, derived for the case when ϕ and P of the filter exactly match with the corresponding cluster functions, are shown as reference in the tables within the small boxes.

The ranges of the filter parameters are clearly far beyond the variations expected for realistic cases. Nevertheless, the results given in Tabs. 1 and 2 illustrate the stabilizing effect of using both spatial and magnitude information to derive the cluster z and Λ_0 . For some parameter combinations, however, the systematic errors are amplified.

It is also seen that false values of the cutoff radius, r_{co} , give larger systematic z and Λ_0 errors compared to false values of the core radius, r_c . One might expect that the stronger effect of r_c on truncated cluster profiles would

also translate into higher sensitivities of z and Λ_0 on this filter parameter. The conclusion, however, neglects the effects of errors in the background number counts. The number of the background galaxies expected for the cluster area scales with r_{co}^2 so that small errors in r_{co} have a large effect.

In many clusters of galaxies the presence of substructures may lead to significant systematic errors in the estimated cluster richnesses and redshifts. In order to simulate unrelaxed clusters in a stage of formation by merging of subunits we approximate such configurations by superposing two cluster models at close separation which seems to describe observed mergers quite well (e.g., Briel et al. 1991, Böhringer et al. 1996). The two components are supposed to have the same redshift and therefore the same number density profiles and luminosity functions, but varying richness ratios are chosen. Tab. 3 summarizes the results obtained for different distances Δr (in units of r_c) between the centers of the two components, and for different ratios, Λ_1/Λ_2 , of the richnesses. The table gives for the combined system the estimated richnesses (numerator) normalized to the richness of the main component, and the estimated redshifts (denominator). As expected, the maximum likelihood filter gives for small Δr the approximate sum of the two richnesses, converging for large Δr to the richness of the main component. Fortunately, the redshifts are almost unaffected by this type of substructure.

The effects of different faint-end slopes of the luminosity functions (not shown here) are significantly smaller compared to the effects mentioned above and can in general be neglected for the distant clusters.

To summarize, the likelihood filter described here, is shown to be a useful method to detect and to characterize distant clusters of galaxies. Clusters with comparatively low richnesses can be detected out to fairly large distances. Reliable redshift and richness estimates, can, however, only be obtained for the more nearby, richer, and isolated systems.

Acknowledgements. Sincere thanks go to H.T. MacGillivray for making the COSMOS galaxy catalogue available to us. We thank the referee, A. Bijaoui, for some useful comments, especially for his idea to study the effects of substructures. P.S. thanks for support by the Verbundforschung under the grant No. 50 OR 9708 35.

References

- Barlow, R.J., 1996, *Statistics* (Chichester: J. Wiley & Sons)
 Brent, R., 1973, *Algorithms for Minimization without Derivatives* (Englewood Cliffs, N.J.: Prentice-Hall)
 Briel, U.G., Henry, J.P., Schwarz, R.A., Böhringer, H., Ebeling, H., Edge, A.C., Hartner, G., Trümper, J., & Voges, W., 1991, *A&A*, 246, L10
 Böhringer, H., Neumann, D.M., Schindler, S., & Kroon-Korteweg, R.C., 1995, *ApJ*, 467, 168
 Colless, M., 1989, *MNRAS*, 2137, 799

- Cressie, N.A.C., 1993, *Statistics for Spatial Data* (New York: J. Wiley & Sons)
 Daley, D.J., & Vere-Jones, D., 1988, *An Introduction to the Theory of Point Processes* (New York: Springer-Verlag)
 Dalton, G.B., Efstathiou, G., Maddox, S.J., & Sutherland, W.J., 1994, *MNRAS*, 269, 151
 Dalton, G.B., Maddox, S.J., Sutherland, W.J., & Efstathiou, G., 1997, *MNRAS*, 289, 263
 de Vaucouleurs, G., de Vaucouleurs, A., Corwin (Jr.), H.G., Buta, R.J., Paturel, G., & Fouqué, 1991, *Third Reference Catalogue of Bright Galaxies, Vol. I*, (New York: Springer-Verlag)
 Dickey, J.M., & Lockman, F.J., 1992, *ARAA*, 28, 215
 Efstathiou, G., Ellis, R.S., & Peterson, B.A., 1988, *MNRAS*, 232, 431
 Guzzo, L., et al. 1995, in *Wide Field Spectroscopy and the Distant Universe*, eds. S.J. Maddox & A. Aragón-Salamanca, (Singapore: World Scientific), 205
 Heydon-Dumbleton, N.H., Collins, C.A., MacGillivray, H.T., 1989, *MNRAS*, 258, 1
 Karr, A.F., 1986, *Point Processes and their Statistical Inference* (New York: Marcel Dekker)
 Kawasaki, W., Shimasaku, K., Doi, M., & Okamura, S., 1998, *AASS*, 130, 567
 Kemperman, J.H.B., 1984, in *Inequalities in Statistics and Probability*, ed. Y.L. Tong, *IMS Monograph Series, Vol. 5*, Institute of Mathematical Statistics, Hayward, CA, 84
 König, D., & Schmidt, V., 1992, *Zufällige Punktprozesse* (Stuttgart: Teubner)
 Layzer, D., 1956, *AJ*, 61, 383
 Lumsden, S.L., Collins, C.A., Nichol, R.C., Eke, V.R., & Guzzo, L., 1997, *MNRAS*, 290, 119
 Metcalfe, N., Shanks, T., Roche, N., & Fong, R., 1993, *Ann. New York Acad. Sci.*, 688, 534
 Neyman, J., 1961, in *Problems of Extragalactic Research*, ed. G.C. McVittie (New York: Macmillan), 294
 Neyman, J., & Scott, E.L., 1952, *ApJ*, 116, 144
 Postman, M., Lubin, L.M., Gunn, J.E., Oke, J.B., Hoessel, J.G., Schneider, D.P., & Christensen, J.A., 1996, *AJ*, 111, 615
 Predehl, P., & Schmitt, J.H.M.M., 1995, *A&A*, 293, 889
 Ripley, B.D., 1991, *Statistical Inference for Spatial Processes* (Cambridge: Cambridge University Press)
 Rubin, I., 1972, *IEEE IT-18*, 547
 Sen, P.K., & Singer, J.M., 1993, *Large Sample Methods in Statistics* (New York: Chapman & Hall)
 Snyder, D.L., 1972, *IEEE Trans. Am. Math. Soc.*, 104, 79
 Snyder, D.L., 1975 *Random Point Processes* (New York: J. Wiley & Sons)
 Stoyan, D., Kendall, W.S., & Mecke, J., 1995, *Stochastic Geometry and its Applications* (Chichester: J. Wiley & Sons)
 Stoyan, D., & Stoyan, H., 1992, *Fraktale - Formen - Punktfelder* (Berlin: Akademie Verlag)
 Yashin, A., 1970, *Automation and Remote Control* 1970, 725

Appendix A: Derivation of Likelihood Functions for Point Processes

In the first step, the probability generating functional G_A of a point process, defined by the expectation

$$G_A[h] := E \left(\prod_{x_i \in \mathbb{N}} h(x_i) \right), \quad (\text{A.1})$$

must be specified (e.g., Stoyan, Kendall, & Meck 1995, p.116). Here, $h(x)$ is a $[0,1]$ -valued (test) function. In (A.1) the point process on A is represented by N , and the points are located at the spatial positions $\{x_i\}$.

In the second step, the logarithmic generating functional obtained with (A.1) is compared with the expansion

$$\ln G_A[h] = -K_0(A) + \sum_{n=1}^{\infty} (n!)^{-1} \int_{A^{(n)}} h(x_1) \cdots h(x_n) K_n(dx_1 \cdots dx_n | A) \quad (\text{A.2})$$

to get the Khinchin measures, K_n . Some remarks concerning the derivations of both equation (A.2) and (A.3, see below) can be found in Daley & Vere-Jones (1988, Sect. 5.5, and p. 230).

In the last step, the K_n measures are inserted into the expansion of the local Janossy densities,

$$j_N(x_1, \dots, x_N | A) = e^{-K_0} \sum_{r=1}^N \sum_{\tau \in \mathcal{P}_{r,N}} \prod_{i=1}^r k_{|S_i(\tau)|}(x_{i,1}, \dots, x_{i,|S_i(\tau)|} | A), \quad (\text{A.3})$$

to get in combination with equation (1) the likelihood function of the point process. The second sum on the right-hand side of (A.3) is taken over all r -partitions $P_{r,N}$ where $|S_i(\tau)|$ gives the number of elements in each partition set.

Example: Inhomogeneous Poisson point process.

For this process, equation (A.1) gives (Cressi 1993, p. 650)

$$\ln G_A[h] = - \int_A (1 - h(x)) \lambda(x) dx. \quad (\text{A.4})$$

With equation (A.2) we obtain the only nonzero Khinchin measures, $K_0 = \int_A \lambda(x) dx$ and $k_1(x|A) = \lambda(x)$, resulting to the Janossy density

$$j_N(x_1, \dots, x_N | A) = e^{-K_0} \prod_{i=1}^N k_1(x_i | A), \quad (\text{A.5})$$

which directly leads to the likelihood function of the inhomogeneous Poisson point process (eq. 2 in Sect. 2.1).

Appendix B: High-Background Approximation

Equations (8) and (9) are mathematically exact and are based on no special mathematical approximation. In this section it will be shown that the equations of the digital filter derived by Postman et al. (1996) – not the finally equations used – can be obtained if

$$b(m) \gg \Lambda \phi(m - m^*) P\left(\frac{r}{r_c}\right). \quad (\text{B.1})$$

In this limit the left side of the condition (9) may be approximated by

$$\sum_{i=1}^N \frac{\phi(m_i - m^*)}{b(m_i)} P\left(\frac{r_i}{r_c}\right) - \Lambda \sum_{i=1}^N \frac{\phi^2(m_i - m^*)}{b^2(m_i)} P^2\left(\frac{r_i}{r_c}\right),$$

from which a closed analytic form for the cluster richness is obtained

$$\Lambda \approx \frac{\sum_{i=1}^N \frac{\phi(m_i - m^*)}{b(m_i)} P\left(\frac{r_i}{r_c}\right) - 1}{\sum_{i=1}^N \frac{\phi^2(m_i - m^*)}{b^2(m_i)} P^2\left(\frac{r_i}{r_c}\right)}. \quad (\text{B.2})$$

In the same limit (8) reduces to

$$\ln\left(\frac{L}{L_0}\right) \approx \Lambda \left(\sum_{i=1}^N \frac{\phi(m_i - m^*)}{b(m_i)} P\left(\frac{r_i}{r_c}\right) - 1 \right). \quad (\text{B.3})$$

Inserting (B.2) into (B.3) gives an analog equation to (8) in the high-background approximation

$$\ln\left(\frac{L}{L_0}\right) \approx \frac{\left(\sum_{i=1}^N \frac{\phi(m_i - m^*)}{b(m_i)} P\left(\frac{r_i}{r_c}\right) - 1 \right)^2}{\sum_{i=1}^N \frac{\phi^2(m_i - m^*)}{b^2(m_i)} P^2\left(\frac{r_i}{r_c}\right)}. \quad (\text{B.4})$$

It is seen that equations (B.4) and (B.2) correspond to equations (15) and (14) in Postman et al. (1996), respectively, if

$$\sum_{i=1}^N \frac{\phi^2(m_i - m^*) P^2\left(\frac{r_i}{r_c}\right)}{b^2(m_i)} \approx \int_A \int_B \frac{\phi^2(m - m^*) P^2\left(\frac{r}{r_c}\right)}{b^2(m)} \lambda(r, m) dm d^2 r \quad (\text{B.5})$$

$$\approx \int_A \int_B \frac{\phi^2(m - m^*) P^2\left(\frac{r}{r_c}\right)}{b(m)} dm d^2 r, \quad (\text{B.6})$$

and

$$\sum_{i=1}^N \frac{\phi(m_i - m^*) P\left(\frac{r_i}{r_c}\right)}{b(m_i)} \approx \int_A \int_B \frac{\phi(m - m^*) P\left(\frac{r}{r_c}\right)}{b(m)} \lambda(r, m) dm d^2 r, \quad (\text{B.7})$$

and the normalization (5) holds.

Appendix C: Median Polish Algorithm

In the present investigation median polishing is used to identify those photographic plates where the surface number density of galaxies deviates significantly from the central plate containing the major part of the galaxy cluster, so that the galaxies on those ‘pathological’ plates can be rejected from further analyses. The algorithm is, however, more powerful and thus interesting enough to be described in more detail. The method can, for example, be used for samples of sufficiently large sizes as a *definition procedure* of stationary point distributions.

Let N_{kl} , $k = 1, \dots, p$; $l = 1, \dots, q$ be the number of points counted in the cell with the indices k and l . The k and the l index may number the count cells along the

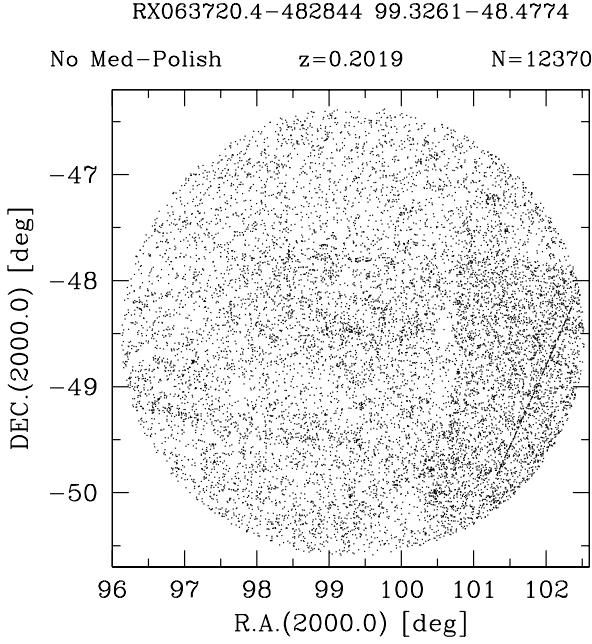


Fig. C.1. Angular distribution of the COSMOS galaxies with $b_J \leq 20.5$ mag centered around the ROSAT X-ray source RX063720.4-482844. The data are collected from four different Schmidt plates. Multiple detections of galaxies in the overlaps of adjoining plates are rejected. The redshift of the central cluster of galaxies is $z = 0.2019$ measured in the course of an ESO Key Programme (Guzzo et al. 1995).

Right Ascension and along the Declination axis, respectively. We follow the terminology of Cressi (1993, p. 186) and define for $i = 1, 3, 5, \dots$,

$$N_{kl}^{(i)} := N_{kl}^{(i-1)} - \text{med}\{N_{kl}^{(i-1)} \mid l = 1, \dots, q\},$$

$$k = 1, \dots, p+1; \quad l = 1, \dots, q, \quad (\text{C.1})$$

$$N_{k,q+1}^{(i)} := N_{k,q+1}^{(i-1)} + \text{med}\{N_{kl}^{(i-1)} \mid l = 1, \dots, q\},$$

$$k = 1, \dots, p+1, \quad (\text{C.2})$$

and define for $i = 2, 4, 6, \dots$,

$$N_{kl}^{(i)} := N_{kl}^{(i-1)} - \text{med}\{N_{kl}^{(i-1)} \mid k = 1, \dots, p\},$$

$$k = 1, \dots, p; \quad l = 1, \dots, q+1, \quad (\text{C.3})$$

$$N_{p+1,l}^{(i)} := N_{p+1,l}^{(i-1)} + \text{med}\{N_{kl}^{(i-1)} \mid k = 1, \dots, p\},$$

$$l = 1, \dots, q+1. \quad (\text{C.4})$$

Here, $\text{med}\{x_1, \dots, x_n\}$ is the median of $\{x_1, \dots, x_n\}$. The algorithm starts with

$$N_{kl}^{(0)} = \begin{cases} N_{kl} & : \quad k = 1, \dots, p; \quad l = 1, \dots, q \\ 0 & : \quad \text{elsewhere.} \end{cases} \quad (\text{C.5})$$

Usually the method converges after three to five iterations.

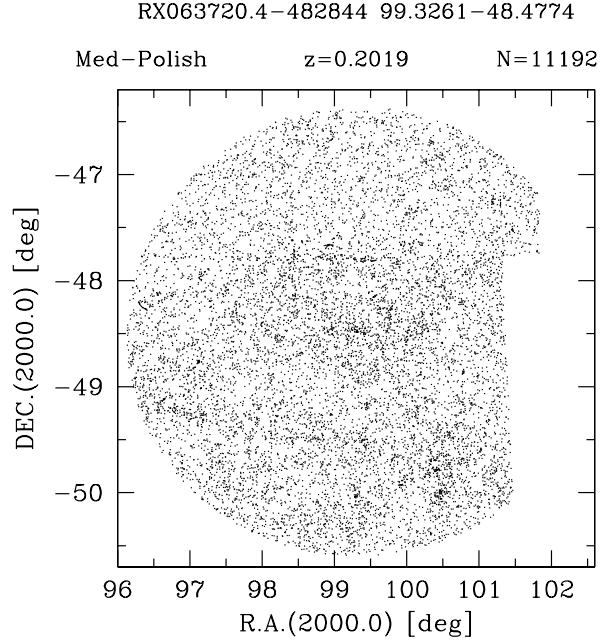


Fig. C.2. As Fig. C.1 after median polishing. The weak indication of a smaller surface number density in the north compared to the south might be attributed to a small error in the magnitude zero-point. Median polishing was adjusted to accept such large-scale deviation from stationarity which are not uncommon in the COSMOS data base. Note that the excised region is smaller than the dark region in Fig. C.1 due to the plate overlap.

After median polishing the original $p \times q$ data matrix is replaced by a $p \times q$ residual matrix, Δ_{kl} , and by the $p + q + 1$ extra elements containing the deviations along the rows, $\{r_k\}$, the deviations along the columns, $\{c_l\}$, and the average background level, $\{a\}$. These quantities are related by

$$N_{kl} = a + r_k + c_l + \Delta_{kl},$$

$$k = 1, \dots, p; \quad l = 1, \dots, q. \quad (\text{C.6})$$

Equation (C.6) shows that a describes the overall median surface number density of galaxies in the area covered by the spatial indices k and l . Correspondingly, the projected median surface number density profile in excess to the global median a along, e.g., the Right Ascension and the Declination axes, is thus given by the r_k and by the c_l vector, respectively. The residual matrix Δ_{kl} gives the remaining deviations from (first-order) stationarity. The three effects are unbiased estimates if the coordinates of the individual galaxies are transformed into equal-area Hammer Aitoff coordinates.

Figures C.1 and C.2 illustrate the performance of the filter. In this example the COSMOS galaxy data of four adjoining Schmidt plates (C.1) are combined. Median polishing detects the artificial inhomogeneity at R.A. > 100.5

degrees, rejects the corresponding data from further analyses, and starts again with a new combination of the COSMOS data from the remaining Schmidt plates (C.2). The algorithm can be regarded as a standard procedure in spatial data analyses and is thus well studied both mathematically and in many practical applications (see the examples and references collected by Cressi 1993).